2023 IEEE/ASME International Conference on Advanced Intelligent Mechatronics (AIM)
June 28-30, 2023. Seattle, Washington, USA

System Identification and Force Estimation of a Grinding Tool

Shang-Ya Siao, Yu-Lin Chu, and Pei-Chun Lin

***Abstract*—Normal force is one of the most important factors in the grinding and polishing process. This project focuses on system identification of the grinding tool Mini Robot, which can not only spin the grinding wheel but also actively control the force along with the shaft direction using a voice coil motor, achieving a fine grinding quality. This advantage can widely benefit many collaboration platforms such as an automation grinding platform with manipulator. System identification of this grinding tool was carried out to build a state observer feedback-control system. The force was estimated using the information on current and displacement of the voice coil motor. Feedback-control design can later be added into the system.**

Keywords——grinding tool, integration of electromechanical system, system identification, force estimation, voice coil motor

I. INTRODUCTION

The grinding process is a necessary step in many manufacturing industries. Products that need a fine surface quality usually need to go through this step before polishing or electroplating because after grinding, the excessive material is removed and the grooves are much smaller, which makes the polishing process more effective. This job was traditionally a time-consuming manual operation, and the noise problem and dust pollution were bad for health. Therefore, over the last few decades, much research has been done to turn this work into automation engineering [1, 2]. An automatic grinding system commonly includes a muti- degree-of-freedom (multi-DOF) robot and a grinder. The muti- DOF robots can be CNC machines [3] or manipulator robots [4, 5], flexible enough to carry out the task of moving and rotating grinding work piece surfaces through the grinders which are either mounted on the muti-degree-of-freedom robot or fixed on a platform.

The grinder category includes different kinds, like belt grinding [4-6] and wheel grinding [7-9]. Many factors that affect the final surface roughness were studied; for example, work speed, wheel speed, grit size, grinding power, and grinding force. Those factors can be optimized through experiment, and the grinding force was proven to be a critical factor. In [10], Durgumahanti et al. used a single-grit test to build a new grinding force model which deconstructed force into friction force, ploughing force, and cutting force. D. Zhu further researched how the ratio of force components changes under different grinding parameter combinations [11], and the conclusion was that having constant contact force combined with optimal process parameters is a good method for grinding complex surfaces.

In some research, the grinding force self-develops once the contact is established and the force is decided by robot compliance. This means that the trajectory planning decided both the grinding area and the grinding force. As a result, the trajectory planning and control became a major goal [12]. A hybrid force/position controller was used [7, 13]. In [7], to achieve turbine blade grinding, the tool paths are divided into vector tangential to the surface for position and vector normal to the surface for normal force. The robot they used was a Scompi robot, which was flexible, so a laser tracker was used to guarantee the trajectory accuracy. There are other ways to compensate the position error. The work in [8] designed a compliance tool including an elastic sponge and a force sensor to keep the normal force within a certain range. Aside from the passive grinding force absorber, there are active force control grinders, as [14, 15] used cushion cylinder and force sensor. Force sensors are widely used in force control systems [5-9]. But force sensors have an issue of hysteresis-induced drift, which causes a larger error in force control. In [16], a way to control the force with frequency analysis rather than directly using the data of force sensors was proposed. Lin et al. designed a control loop to mix the force sensor data with a force prediction model [17]. The aforementioned is force prediction research, but a real-time force output estimation aimed at the active force control actuator is more suitable for complex surface grinding tasks.

In this project, we used a grinder with voice coil motor as an active force control actuator. During grinding experiments, the phenomenon of hysteresis-induced drift of force sensor caused by the coil current changing of VCM occurred. Besides, the force sensor sensed a large overshoot at the moment of contact. Based on the force data, this overshoot caused the force controller to generate unstable oscillations. Therefore, we built a state observer feedback control system to estimate the normal force through other sensors. The advantages of VCM include high-speed response; the normal force produced by VCM could be controlled through the coil current [18], and the small displacement won't cause the output force to change, which means the tolerance for position error increases [19]. For the purpose of fully controlling the normal force during the grinding process, system model identification was done. More controllers can be added in the future.

The remainder of this work is described as follows. The grinding robot system description and dynamic model are described in section II. Section III is about system model identification and section IV showed the model identification results with simulation. The conclusion is section V.

This work is supported by National Science and Technology Council (NSTC), Taiwan, under contract MOST 111-2634-F-007-010- and National Taiwan University, Taiwan, under contract NTU-CC-112L890604.

The authors are with Department of Mechanical Engineering, National Taiwan University (NTU), No.1 Roosevelt Rd. Sec.4, Taipei 106, Taiwan. (Corresponding email: peichunlin@ntu.edu.tw).

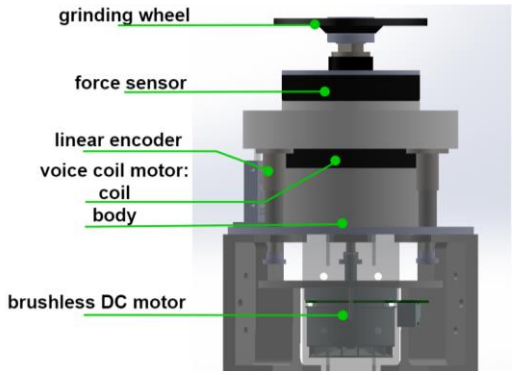

Fig. 1. CAD drawing of the designed grinding tool.

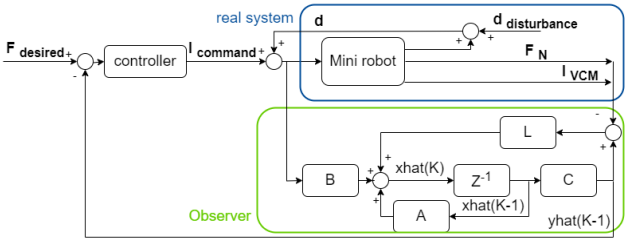

Fig. 2. Control block diagram of the grinding tool.

II. GRINDING ROBOT SYSTEM AND DYNAMIC MODEL

A. Mechanism and control system of grinding tool

The grinding tool used in this project was Mini Robot. The design and mechanism are described in [9]. The differences between the old version and new version of Mini robot are the brushless DC motor and some structure, as Fig.1 shows. The equipment of Mini robot is shown in TABLE I.

To construct a state observer feedback-control system as shown in Fig.2, three states needed to be included, which are: the coil current of the voice coil motor, the displacement of the coil, and the normal force applied to the grinding work piece. Some research didn't consider the first two states together when doing the force control of voice coil motor and still got good results of VCM control as vibration absorbers [20], but in order to achieve a precise control based on our electromechanical system, the first two states are necessary. The necessities are explained in the following section.

TABLE I. COMPONENTS OF THE GRINDING TOOL

name	Equipment of grinding system		
	brand	***model***	***usage***
Controller	National instruments	PXI - 7852R R Series Multifunction Device	Control actuators and collect data
Voice coil motor	moticont	HVCM-095-038-051-01	Linear actuator
BLDC motor	maxon	EC60fl. (614949) + enc MILE (651156)	Rotary actuator
Linear encoder	celeramotion	VIA-1000-AA0-20-30A	Displacement sensor
Servo controller	Maxon	ESCON 70/10, ESCON Module50/8He	Motor driver
Force sensor	Sunrise Instruments	M3705C	6-axis force/torque sensor

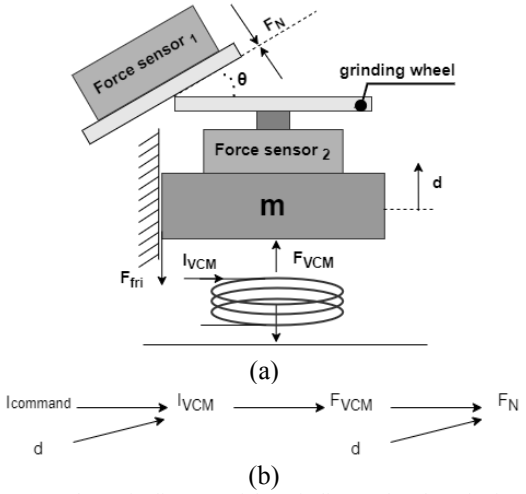

Fig. 3. (a) Schematic diagram of the grinding tool and work piece and (b) relationship of the parameters for identification.

B. Grinding system dynamic model

The basic principle of the voice coil motor is the magnetic effect of electric current: the magnetic field created by the coil current interacts with the permanent magnet's magnetic flux, inducing the force [21]. The force can be calculated by:

$$F_{VCM} = K_F(d) I_{VCM} \tag{1}$$

F_{VCM} represents the induced force. $K_F(d)$ is the force constant, which changes according to the position of the coil because the permanent magnet's magnetic flux varies in different places. I_{VCM} is the coil current. In this work, $K_F(d)$ is assumed to be constant due to the small displacement occurring in the grinding process. The equivalent circuit of voice coil motor from an electrical point of view:

$$E_{VCM} = R I_{VCM} + L \frac{dI_{VCM}}{dt} + K_B V \tag{2}$$

E_{VCM} is the applied voltage. R and L represent the equivalent resistance and inductance. V is the coil's moving speed, which is the derivative of the displacement to time. K_B is the back electromotive force constant. Equation (1) shows that F_{VCM} is only influenced by I_{VCM}, while (2) indicates that I_{VCM} is influenced by V and E_{VCM}.

The Mini robot dynamic model is shown in Fig.3(a). Fig.3(b) shows the interaction between states. d and F_N are the displacement of the coil and the normal component of grinding force, which are included in the control system states. θ is the tilt angle. F_{fri} is the kinetic friction and $F_{acc} = \mathrm{m} \cdot \ddot{d}$. The relation between F_{VCM} and F_N can be expressed as:

$$\left(F_{VCM} - mg - F_{acc} \pm F_{fri}\right) \times \cos\theta = F_N \tag{3}$$

III. MODEL IDENTIFICATION OF GRINDING SYSTEM

In this project the states that can be observed by sensors are I_{VCM}, d, and F_N. At first, F_N was collected from $Force\ sensor_2$, which was mounted on Mini robot, but the

force data were affected by I_{VCM}. As a result, an extra force sensor was added behind the grinding work piece. F_N in the following experiments were measured by Force sensor_1. The current control is achieved by the usage of the ESCON servo controller. In the current control operating mode, E_{VCM} is adjusted automatically. Equation (2) shows that when V changes rapidly, E_{VCM} needs to change correspondingly. If the rate of change exceeds the limit of ESCON, it will produce a difference between I_{VCM} and $I_{command}$.

The model identification was composed of two experiments' results. The first experiment was designed for the purpose of finding the transfer function with I_{VCM} as the input and F_N as the output. According to (1), (2), and (3), if d is fixed, F_N will be only influenced by I_{VCM}. The second experiment was designed for the purpose of finding the transfer function with d as the input and I_{VCM} as the output.

A. Model identification experiment

Fig.4 shows the experimental platform. PUU3T is a parallel manipulator which can provide a regular displacement. A force sensor was mounted on the end-effector of PUU3T, which served as the force sensor 1 in Fig.3(a). shows the experiment set-up of command input and the corresponding sensor data output. The sampling rate of the system was 1000Hz. The movable range of displacement is 2.5mm~7mm. The lower bound and upper bound are constrained by rubber gaskets.

The ω_1 applied in the first experiment (EXP #1) contains: 0.1, 0.2, 0.5, 1, 2, 3, 4, 5, 6, 7, 8, 9, 10, 11, 12, 13, 14, 15, 16, 17, 18, 19, 20, 22.2, 25, 28.6, 30, 31, 32, 33, 34, 36, 37, 38, 40, 42, 43, 45, 47, 50, 52, 55, 58, 62, 66, 71, 76, 83, 90, 100, 111, 125, 142, 166, 200 (Hz). In the experiment process, d was fixed at near 6 mm, where the voice coil motor has a better force constant. The sinusoidal waves of I_{VCM} were controlled by $I_{command}$.The ω_2 applied in the first experiment (EXP #2) contained: 0.2, 0.5, 1, 2, 3, 4, 5, 6, 7, 8, 9, 10, 11, 12, 13, 14, 15 (Hz). In the experiment process, $I_{command}$was fixed at 1.48 A. The sinusoidal waves of d were produced by PUU3T and the sinusoidal waves' centers were 6mm. The combination result of those two experiments is the model's identification at $I_{VCM} = 14.8\ A,\ d = 6\ mm$.The upper bound of ω_2 was set due to the requirement of consistency. The greater the ω_2, the higher the acceleration, and F_{acc} goes up. If F_{acc} increased, the corresponding F_N decreased. When F_N is too small, Mini robot and PUU3T will lose contact occasionally. A simple solution is increasing the value of $I_{command}$, but the ideal F_N in the grinding process is around 5N ~15N. The other improvement solutions are discussed in section V .

B. Model construction

In this project, model identification applied the frequency domain method [22].

$$\mathrm{Y}(\omega) = \mathrm{H}(\omega)\mathrm{U}(\omega) \rightarrow \mathrm{H}(\omega) = \frac{Y(\omega)}{U(\omega)} \qquad (4)$$

If the input series was a single frequency sinusoid wave, the output response should be a single frequency sinusoid wave with amplitude $|H(\omega)|$ and phase shift $\angle\mathrm{H}(\omega)$. The time series data were transformed to frequency domain by FFT. One of the

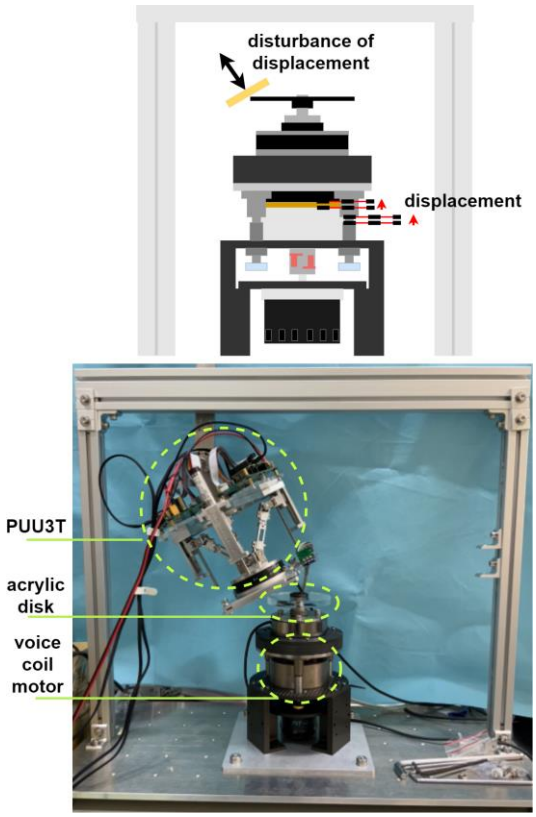

Fig. 4. A schematic diagram and a photo of the experimental platform. The grinding wheel was replaced by an acrylic disk in the photo.

advantages of sinusoid sweep is that the white noise influence can be ignored because only the target frequency data will be used.

In the process of the first experiment, a phenomenon similar to natural frequency happened. The resonant frequencies are at 13 Hz and 45Hz, as Fig.5 shows. It indicated that there were at least two pair of complex conjugate poles. As a result, when doing transfer function estimation, the main focus was on resonant frequencies, and the zeros number was determined according to the phase shift at high frequencies.

The transfer function from $I_{command}\ to\ I_{VCM}$ $\left(G_{I_{command}\ to\ I_{VCM}}\right)$ and the transfer function from $I_{command}\ to\ F_{VCM}$ $\left(G_{I_{command}\ to\ F_{VCM}}\right)$ were built from the data of the first experiment. Using $G_{I_{command}\ to\ F_{VCM}}$, mg could be calculated from the difference between F_N and F_{VCM} by a constant $I_{command}$ and a fixed displacement. From the data collected in the second experiment, the assumption that when the rate of V change (acceleration) exceeds the limit of ESCON, there will be a difference between I_{VCM} and $I_{command}$ was confirmed. Fig.6(a) shows that the second derivative of the displacement to time affects I_{VCM} because the accelerations at each frequency are quadratic in frequencies. That is to say the acceleration value at different frequencies have a ratio of:

$0.2^2, 0.5^2, 1^2, 2^2, 3^2, 4^2, 5^2, 6^2, 7^2, 8^2, 9^2, 10^2, 11^2, 13^2, 14^2,$

15^2. The magnitudes of $I_{VCM}/displacement$ are also quadratic in frequencies. The acceleration value was computed

from displacement by Newton interpolation formula and a lowpass filter with passband frequency at 40Hz.

TABLE II. PARAMETER SET-UP IN THE EXPERIMENT

	Experiment set-up	
	Input	***output***
EXP #1	$I_{command} = 0.064 \cdot sin(2\pi\omega_1 t) + 1.48\ (A)$ $d = 5500, 6000, 6500(\text{um})$	I_{VCM}
EXP #2	$d = 200 \cdot \sin(2\pi\omega_2 t) + 6000(\text{um})$	I_{VCM}

The transfer function from *displacement* to I_{VCM} ($G_{d\ to\ I_{VCM}}$) was built up by the transfer functions from acceleration to I_{VCM} ($G_{acc\ to\ I_{VCM}}$) and the transfer functions of second derivative (G_{s^2}), as Fig.6 (b) show. The discrete time transfer functions of derivative are unstable. The Zero Phase Error Tracking Algorithm was applied to get a stable result [23]. In order to obtain F_N, F_{acc} and F_{fri} need to be estimated. The data of F_{acc} and F_{fri} couldn't be observed directly from sensor data; therefore, in this project the two of them were calculated from :

$$F_N + mg - F_{VCM} = -F_{acc} \pm F_{fri} \qquad (5)$$

According to Newton's second law of motion, $F_{acc} = \mathrm{m} \cdot \ddot{d}$, which should estimate the F_{acc} accurately. But the acceleration was computed from d, which might amplify high frequency noise, and the F_{fri} *was* still not included. The transfer function from *displacement* to F_{acc} ($G_{d\ to\ F_{cacc}}$) was built in the same way as $G_{d\ to\ I_{VCM}}$, combining the transfer function from *acceleration* to F_{acc}($G_{acc\ to\ F_{acc}}$) and G_{s^2}. The accuracy of the $G_{d\ to\ F_{acc}}$ result was compared with the $F_{acc} = \mathrm{m} \cdot \ddot{d}$ result in section Ⅳ.

TABLE I listed each discrete time transfer function built in the two experiments, which can be combined into a state space model as Fig.2. showed. The time delay order was given according to the phase delay of frequency data and time series data.

TABLE III. TRANSFER FUNCTIONS OF THE IDENTIFIED MODELS

Model name	**Model transfer function estimation**	
	transfer function	***output / input***
$G_{I_{command}\ to\ I_{VCM}}$	$z^{-2}\dfrac{0.0683z^{-1}}{1-1.449z^{-1}+0.517z^{-2}}$	$\dfrac{I_{VCM}(A)}{I_{command}(A)}$
$G_{I_{command}\ to\ F_{VCM}}$	$\dfrac{0.05585z^{-1}-0.1163z^{-2}+0.005312z^{-3}+0.08524z^{-4}}{1-3.664z^{-1}+5.126z^{-2}-3.242z^{-3}+0.7818z^{-4}}$	$\dfrac{F_{VCM}(N)}{I_{command}(A)}$
G_{s^2}	$\dfrac{5e^5z^3-5e^5z^2-5e^5z+5e^5z}{z^3}$	$\dfrac{1}{(sec^2)}$
$G_{d\ to\ F_{acc}}$	$m * G_{s^2} * 10^{-6}$	$\dfrac{F_{acc}(N)}{\mathrm{d}(um)}$
$G_{d\ to\ I_{VCM}}$	$z^{-1}\dfrac{3.552e^{-9}}{1-0.878z^{-1}} * G_{s^2}$	$\dfrac{I_{VCM}(A)}{d\ (um)}$

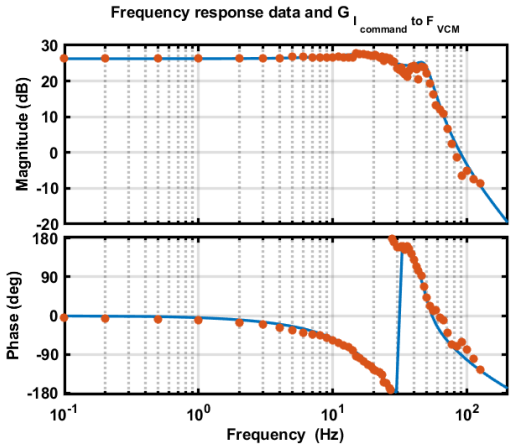

Fig. 5. Fast Fourier Transform results of the first experiment data. Magnitudes and phases of F_{VCM}/I_{VCM} and bode plot of $G_{I_{VCM}\ to\ F_{VCM}}$

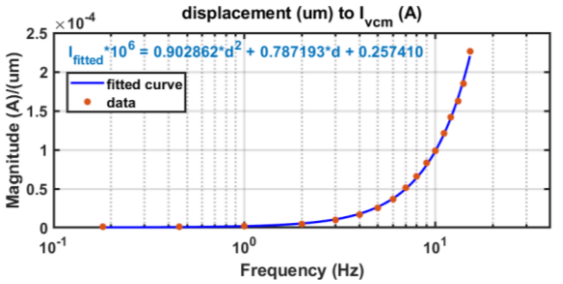

(a)

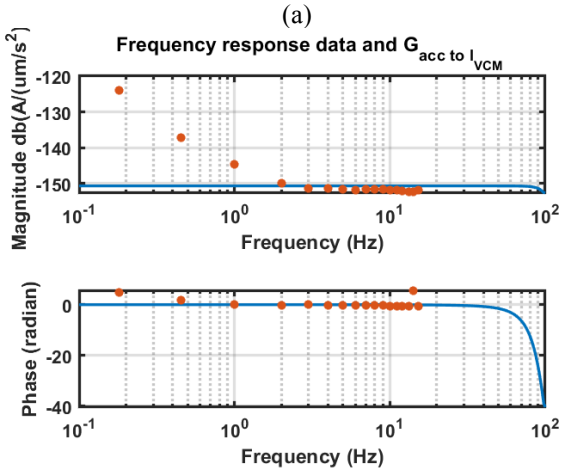

(b)

Fig. 6. Fast Fourier Transform results of the second experiment data. (a)Magnitudes of I_{VCM}/displacement and the fitted curve. (b) Magnitudes and phases of I_{VCM}/acceleration and bode plot of $G_{acc\ to\ I_{VCM}}$

IV. MODEL IDENTIFICATION RESULTS AND COMPARISONS

The states d, I_{VCM}, and F_N could be observed from the sensors. The d state was not controllable and was mainly affected by output disturbance during the experiments and the grinding process. Therefore, the states I_{VCM} and F_N were considered as the reference of the validation.

A. Simulation of I_{VCM} and F_N estimation

The accuracy of the identified model was shown in Fig.7.

I_{VCM} estimation error:
$I_{VCM} - \left(G_{I_{command}to\ I_{VCM}} * I_{command} + G_{d\ to\ I_{VCM}} * d\right)$.
F_N estimation error:
simulation #1 error:
$F_N - \left(G_{I_{VCM}\ to\ F_{VCM}} * I_{VCM} - G_{d\ to\ F_{acc}} * d - mg\right)$
simulation #2 error:
$F_N - [G_{I_{VCM}\ to\ F_{VCM}} * (G_{I_{command}to\ I_{VCM}} * I_{command} + G_{d\ to\ I_{VCM}} * d) - G_{d\ to\ F_{acc}} * d - mg]$

Estimated I_{VCM} had great accuracy at each frequency in simulation. However, if the model is implemented in the real system, a low pass filter should be added due to the G_{s^2}'s property of high pass. The high pass property can be observed from Fig.7(a). The estimated error increases at higher frequencies.

As for the F_N, there are two simulation results. All of them used $G_{I_{VCM}\ to\ F_{VCM}}$ to estimate F_{VCM}, simulation #1 use the current data as I_{VCM} directly, and simulation #2 use $G_{I_{command}to\ I_{VCM}}$ and $G_{acc\ to\ I_{VCM}} * G_{s^2}$ to estimate I_{VCM}. Besides, F_{acc} were estimated with $G_{d\ to\ F_{acc}} * d$ in simulation #1 and simulation #2. From Fig.7, simulation #1 and simulation #2 had similar accuracy. In I_{VCM} error of estimation, it is shown that using $G_{I_{command}to\ I_{VCM}}$ and $G_{d\ to\ I_{VCM}}$ to estimate I_{VCM} can get precise estimation. Even if the estimated I_{VCM} were used as the input of $G_{I_{VCM}\ to\ F_{VCM}}$, it can get similar results as using current data.

In F_N estimation error, simulations#2 is slightly better than simulations#1 and the NRMSE are similar at all frequencies. From the data collected at different frequencies and the estimation results, there were two different possible factors that made it such that F_N couldn't be fully calculated by linear form.

The force F_N (N) and displacement (um) of experimental and force F_N (N) of estimated and versus time of the grinding tool demonstrated in Fig.8. Blue lines are experimental F_N (N). Purple lines are estimated F_N (N) and orange lines are experimental displacement (um). Each figure shows how did the F_N (N) change in the process of the grinding tool vibration at different frequency. The frequency of vibration can be observed from displacement: $d' = 200 \cdot \sin(2\pi\omega t)$ (um), (a) $\omega = 0.5$Hz, (b) $\omega = 10$Hz, (c) $\omega = 14$Hz, where $d' = d - 6000$ (um).

1) F_{fri} was ignored: The value of F_{fri} can be calculated but it needs moving direction information. From Fig.8 (a), the data of F_N varied with the displacement. When displacement decreased, the value of F_N increased, and vice versa. At lower frequencies, the acceleration and I_{VCM} didn't differ much, so the simulation result of the estimated model didn't change.

2) Backlash of the hardware: At the peaks of sinusoid waves, which were when the moving direction changed, the profile of F_N changed. The contact surfaces between PUU3T and Mini robot are small, and the sliding between them causes the touching area moves on the surface. The backlash of the hardware then produced some force disturbance into F_N. The different shape at peaks and troughs shown by Fig.8(b) and (c) could demonstrate the nonlinearity of this phenomenon.

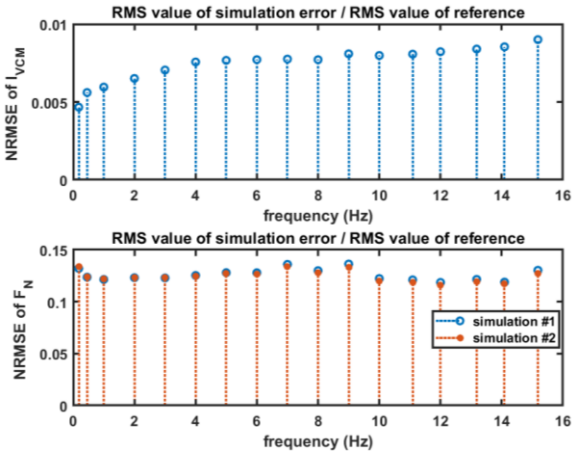

Fig. 7. Simulation results of estimated model.

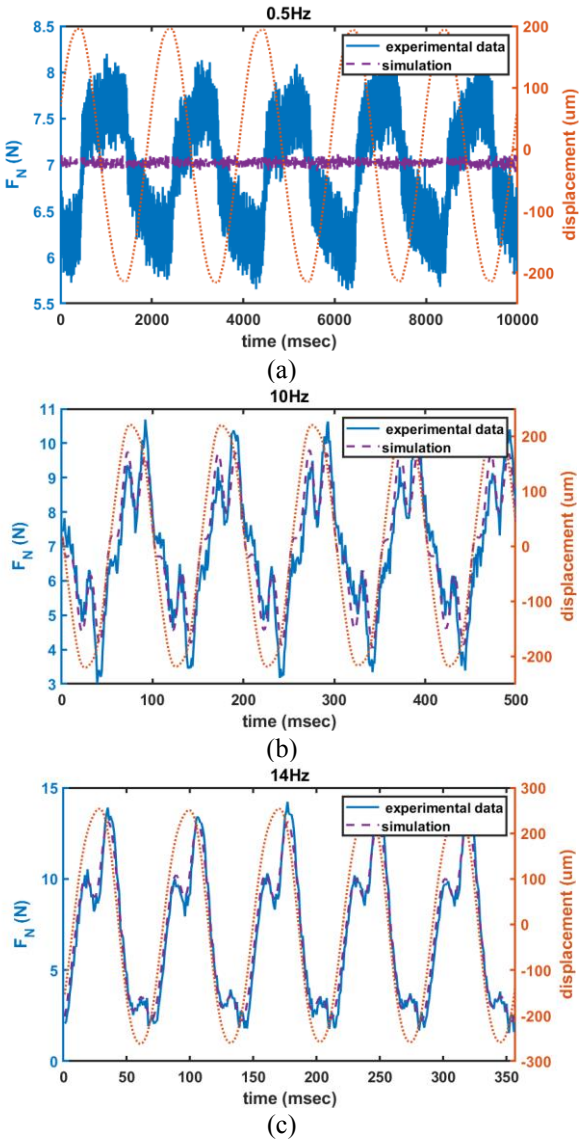

Fig. 8. The force F_N (N) and displacement (um) of experimental and force F_N (N) of estimated and versus time of the grinding tool with different frequencies: (a) $\omega = 0.5$Hz, (b) $\omega = 10$Hz, (c) $\omega = 14$Hz, where $d' = 200 \cdot \sin(2\pi\omega t)$ (um).

V. Conclusion and Future Work

This project focused on completing a grinding system, which can control the normal force during grinding. Because of the hysteresis-induced drift of force sensor caused by the coil current changing of VCM, a force estimation was made. The model identification of the grinding tool system was completed to build a state observer feedback-control system. Through two experiments, which were designed based on the characteristic of voice coil motor, the transfer functions between each state were constructed.

There are many improvements that can be made. According to simulation results, nonlinear force, like friction and deformation, exist. The upper bound of the second experiment was 15Hz, which is a rather low frequency compared with the fundamental frequency of vibration corresponding to grinding wheel rotational speed [15]. The solution might be lightening the structure, but the stiffness of the grinding tool needs to be considered at the same time.

Except for the experiment side, more control design can be added into the control loop through an internal model [20] in the future, such as a repetitive controller which can deal with periodic disturbance[24]. Or a notch filter that can cancel the specific frequency vibration. Due to the characteristic of voice coil motor, Mini robot has higher tolerance for position error. This is a big advantage for collaboration platforms because a muti-degree-of-freedom robot sometimes lacks stiffness.

References

[1] W.-L. Zhu and A. Beaucamp, "Compliant grinding and polishing: A review," *International Journal of Machine Tools and Manufacture,* vol. 158, p. 103634, 2020/11/01/ 2020, doi: https://doi.org/10.1016/j.ijmachtools.2020.103634.

[2] D. Zhu *et al.*, "Robotic grinding of complex components: A step towards efficient and intelligent machining – challenges, solutions, and applications," *Robotics and Computer-Integrated Manufacturing,* vol. 65, p. 101908, 2020/10/01/ 2020, doi: https://doi.org/10.1016/j.rcim.2019.101908.

[3] C. H. Liu, A. Chen, C. C. A. Chen, and Y.-T. Wang, "Grinding force control in an automatic surface finishing system," *Journal of Materials Processing Technology,* vol. 170, no. 1, pp. 367-373, 2005/12/14/ 2005, doi: https://doi.org/10.1016/j.jmatprotec.2005.06.002.

[4] X. Xie and L. Sun, "Force control based robotic grinding system and application," in *2016 12th World Congress on Intelligent Control and Automation (WCICA)*, 12-15 June 2016 2016, pp. 2552-2555, doi: 10.1109/WCICA.2016.7578828.

[5] X. Xu, W. Chen, D. Zhu, S. Yan, and H. Ding, "Hybrid active/passive force control strategy for grinding marks suppression and profile accuracy enhancement in robotic belt grinding of turbine blade," *Robotics and Computer-Integrated Manufacturing,* vol. 67, p. 102047, 2021/02/01/ 2021, doi: https://doi.org/10.1016/j.rcim.2020.102047.

[6] X. Xu, D. Zhu, H. Zhang, S. Yan, and H. Ding, "Application of novel force control strategies to enhance robotic abrasive belt grinding quality of aero-engine blades," *Chinese Journal of Aeronautics,* vol. 32, no. 10, pp. 2368-2382, 2019/10/01/ 2019, doi: https://doi.org/10.1016/j.cja.2019.01.023.

[7] M. Sabourin, F. Paquet, B. Hazel, J. Côté, and P. Mongenot, "Robotic approach to improve turbine surface finish," in *2010 1st International Conference on Applied Robotics for the Power Industry*, 5-7 Oct. 2010 2010, pp. 1-6, doi: 10.1109/CARPI.2010.5624446.

[8] F. Tian, C. Lv, Z. Li, and G. Liu, "Modeling and control of robotic automatic polishing for curved surfaces," *CIRP Journal of Manufacturing Science and Technology,* vol. 14, pp. 55-64, 2016/08/01/ 2016, doi: https://doi.org/10.1016/j.cirpj.2016.05.010.

[9] Y.-H. Lin, M.-W. Liu, and P.-C. Lin, "Development of a Grinding Tool with Contact-Force Control Capability," *Electronics*, vol. 11, no. 5, doi: 10.3390/electronics11050685.

[10] U. S. Patnaik Durgumahanti, V. Singh, and P. Venkateswara Rao, "A New Model for Grinding Force Prediction and Analysis," *International Journal of Machine Tools and Manufacture,* vol. 50, no. 3, pp. 231-240, 2010/03/01/ 2010, doi: https://doi.org/10.1016/j.ijmachtools.2009.12.004.

[11] D. Zhu, X. Xu, Z. Yang, K. Zhuang, S. Yan, and H. Ding, "Analysis and assessment of robotic belt grinding mechanisms by force modeling and force control experiments," *Tribology International,* vol. 120, pp. 93-98, 2018/04/01/ 2018, doi: https://doi.org/10.1016/j.triboint.2017.12.043.

[12] Y. Sun, D. J. Giblin, and K. Kazerounian, "Accurate robotic belt grinding of workpieces with complex geometries using relative calibration techniques," *Robotics and Computer-Integrated Manufacturing,* vol. 25, no. 1, pp. 204-210, 2009/02/01/ 2009, doi: https://doi.org/10.1016/j.rcim.2007.11.005.

[13] F. Nagata *et al.*, "Basic performance of a desktop NC machine tool with compliant motion capability," in *2008 IEEE International Conference on Mechatronics and Automation*, 5-8 Aug. 2008 2008, pp. 83-88, doi: 10.1109/ICMA.2008.4798730.

[14] X. Zhang, H. Chen, N. Yang, H. Lin, and K. He, "A structure and control design of constant force polishing end actuator based on polishing robot," in *2017 IEEE International Conference on Information and Automation (ICIA)*, 18-20 July 2017 2017, pp. 764-768, doi: 10.1109/ICInfA.2017.8079007.

[15] K. Seki, Y. Shinohara, M. Iwasaki, H. Chinda, and M. Takahashi, "High precision force control of pneumatic cylinders considering disturbance suppression with specific frequency," in *2011 IEEE International Conference on Mechatronics*, 13-15 April 2011 2011, pp. 937-942, doi: 10.1109/ICMECH.2011.5971251.

[16] Y. Nogi, S. Sakaino, and T. Tsuji, "Force Control of Grinding Process Based on Frequency Analysis," *IEEE Robotics and Automation Letters,* vol. 7, no. 2, pp. 3250-3256, 2022, doi: 10.1109/LRA.2022.3146578.

[17] S. Lin, Q. Wang, Z. Jiang, and Y. Yin, "Online force control of large optical grinding machine for brittle materials assisted by force prediction," *Proceedings of the Institution of Mechanical Engineers, Part B: Journal of Engineering Manufacture,* vol. 234, no. 1-2, pp. 14-26, 2020/01/01 2019, doi: 10.1177/0954405419841523.

[18] Y. Fujii and S. Hashimoto, "Evaluation of the dynamic properties of a Voice Coil Motor (VCM)," in *2007 14th International Conference on Mechatronics and Machine Vision in Practice*, 4-6 Dec. 2007 2007, pp. 57-61, doi: 10.1109/MMVIP.2007.4430715.

[19] Y. Fujii, K. Maru, and T. Jin, "Method for evaluating the electrical and mechanical characteristics of a voice coil actuator," *Precision Engineering,* vol. 34, no. 4, pp. 802-806, 2010/10/01/ 2010, doi: https://doi.org/10.1016/j.precisioneng.2010.04.003.

[20] C. Yi-De, F. Chyun-Chau, and T. Pi-Cheng, "Application of voice coil motors in active dynamic vibration absorbers," *IEEE Transactions on Magnetics,* vol. 41, no. 3, pp. 1149-1154, 2005, doi: 10.1109/TMAG.2004.843329.

[21] Y. Hirano, J. Naruse, and R. Tsuchiyama, "Dynamic characteristics of a voice coil motor for a high performance disk drive," *IEEE Transactions on Magnetics,* vol. 25, no. 4, pp. 3073-3075, 1989, doi: 10.1109/20.34373.

[22] R. Pintelon and J. Schoukens, *System identification: a frequency domain approach*. John Wiley & Sons, 2012.

[23] M. Tomizuka, "Zero Phase Error Tracking Algorithm for Digital Control," *Journal of Dynamic Systems, Measurement, and Control,* vol. 109, no. 1, pp. 65-68, 1987, doi: 10.1115/1.3143822.

[24] T. Mi-Ching and Y. Wu-Sung, "Design of a plug-in type repetitive controller for periodic inputs," *IEEE Transactions on Control Systems Technology,* vol. 10, no. 4, pp. 547-555, 2002, doi: 10.1109/TCST.2002.1014674.